Light- and strange-quark mass dependence of the $\rho(770)$ meson revisited

R. Molina[(1)] and J. Ruiz de Elvira[(2)]

(1) UNIVERSIDAD COMPLUTENSE MADRID

(2) UNIVERSITÄT BERN

Table of contents

1. Previous results with UChPT
2. Inverse Amplitude Method
3. Results
4. Conclusions

Previous results with UChPT

Previous results with UChPT

UChPT (NLO), Oller, Oset, Pelaez (1999)

$$T = [I - VG]^{-1} V,$$
$$V = [1 - V_4 (V_2)^{-1}]^{-1} V_2$$

Energy levels in the box:

$$\boxed{\det(I - V\tilde{G}) = 0}$$

One-channel, finite $\Longrightarrow$ inf. volume $T = (\tilde{G}(E_i) - G(E_i))^{-1}$

M. Döring, U. G. Meißner, E. Oset and Rusetsky, EPJA (2011)

Analyses done in Refs. : B. H, R. Molina, M. Döring and A. Alexandru, Phys. Rev. Let. 117 (2016),D. Guo, A. Alexandru, R. Molina and M. Döring, Phys. Rev. D(2016) ;Hu, B. and Molina, R. and Doring, M. and Mai, M. and Alexandru, A., Phys. Rev. D (2017)

$N_f = 2$ Lattice data

- D. Guo, A. Alexandru, R. Molina and M. Döring, Phys. Rev. D94 (2016)
- G. S. Bali et al . [RQCD Collaboration], Phys. Rev. D93 (2016)
- M. Göckeler et al. [QCDSF Collaboration], PoS LATTICE (2008)
- C. B. Lang, D. Mohler, S. Prelovsek and M. Vidmar, Phys.Rev.D83 (2011)
- S. Aoki et al. [CP-PACS Collaboration], Phys. Rev. D76 (2007)

Previous results with UChPT

$N_f = 2 + 1$ Lattice data

- D. J. Wilson, R. A. Briceño, J. J. Dudek, R. G. Edwards, and C. E. Thomas, Phys. Rev. D92 (2015)
- J. J. Dudek et al. Phys. Rev. D87 (2013)
- J. Bulava, B. Fahy, B. Hörz, K. J. Juge, C. Morningstar and C. H. Wong, Nucl. Phys. B910 (2016)
- J. Bulava, B. Hörz, B. Fahy, K. J. Juge, C. Morningstar and C. H. Wong, PoS LATTICE (2016)
- S. Aoki et al., Phys. Rev. D84 (2011)
- C. Alexandrou et al., Phys. Rev. D96 (2017)
- Z. Fu and L. Wang, Phys. Rev. D94 (2016)

Previous results with UChPT

SU(2) vs. SU(3)

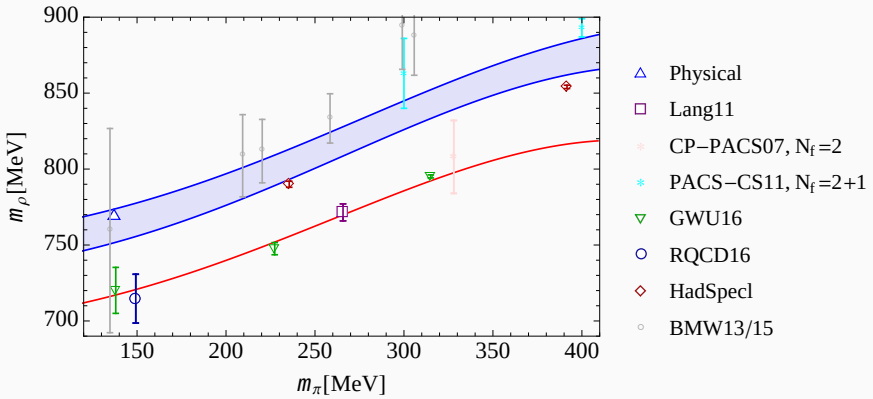

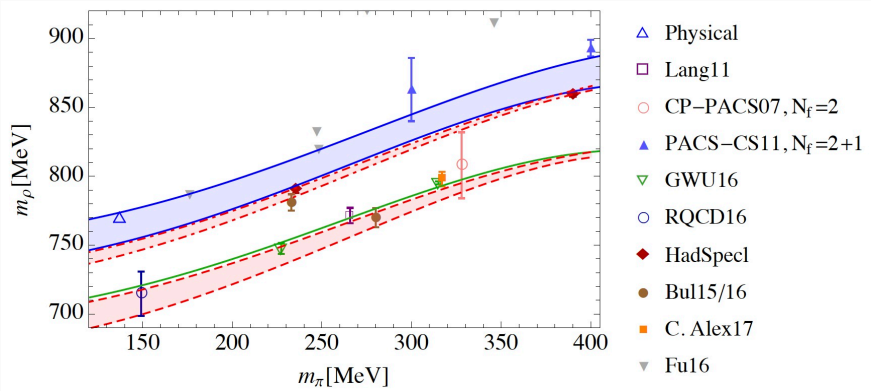

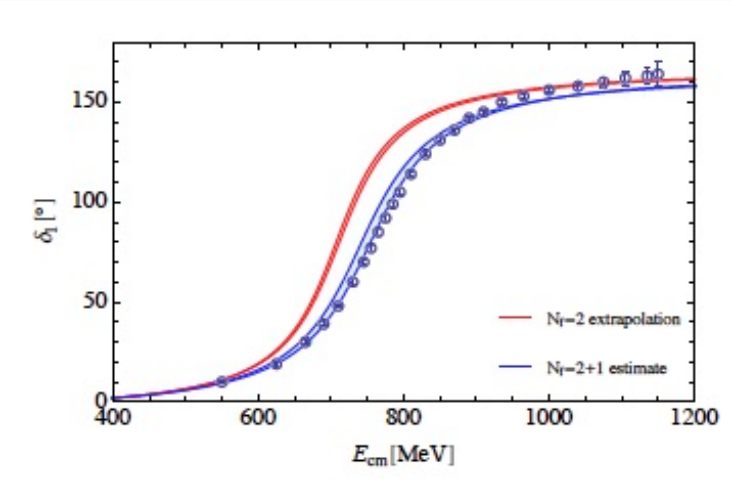

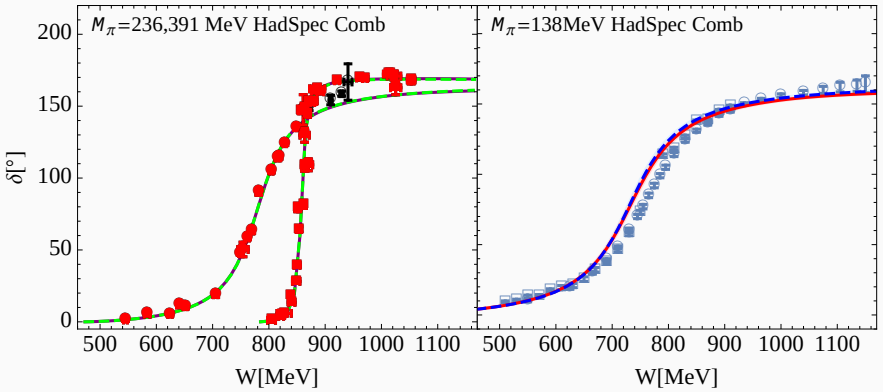

Previous results with UChPT

SU(2) vs. SU(3)

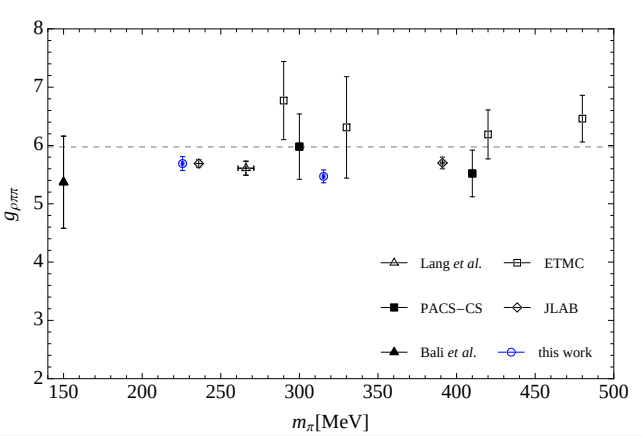

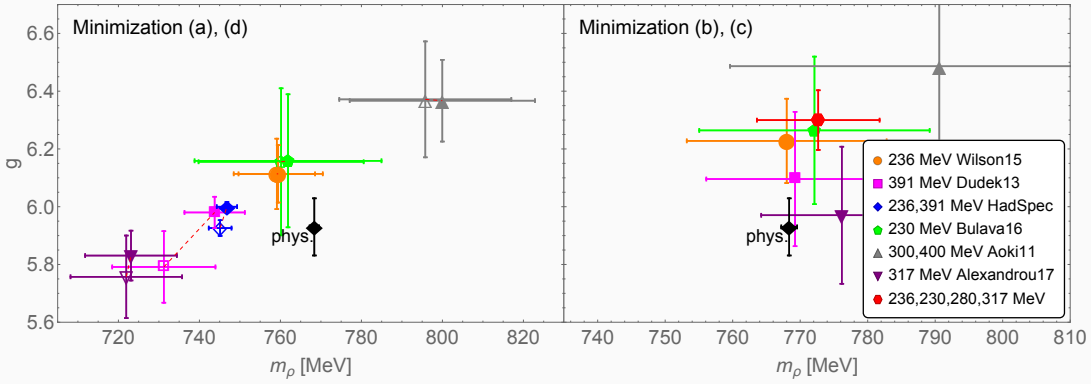

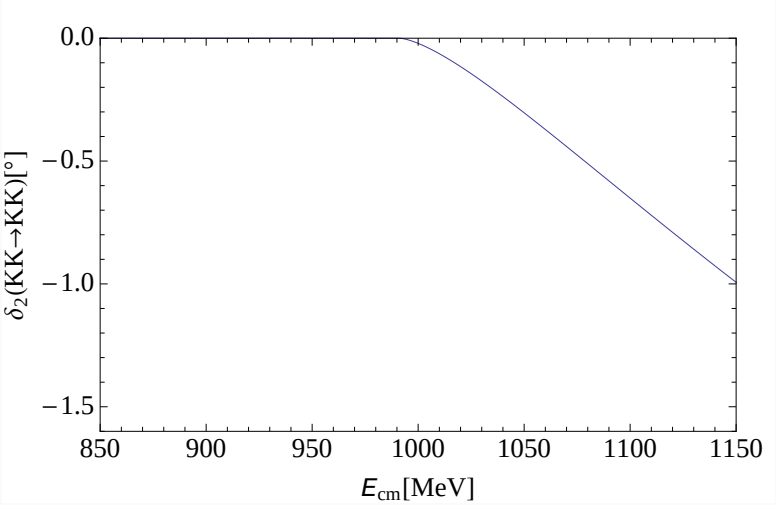

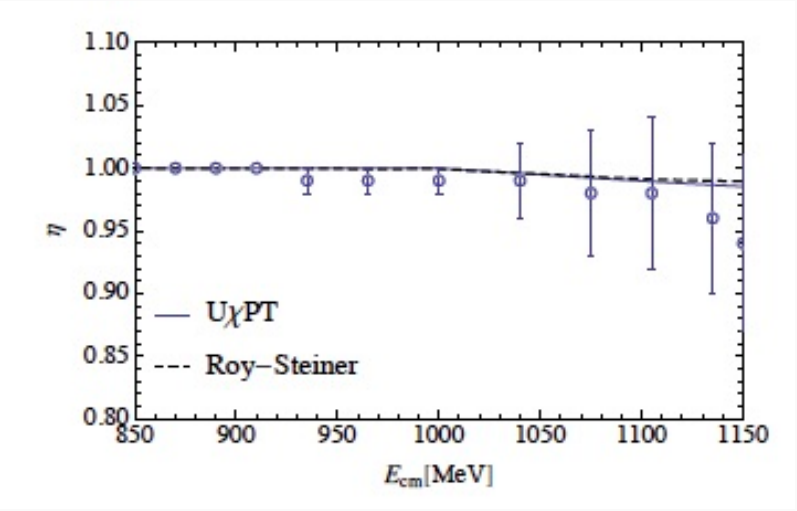

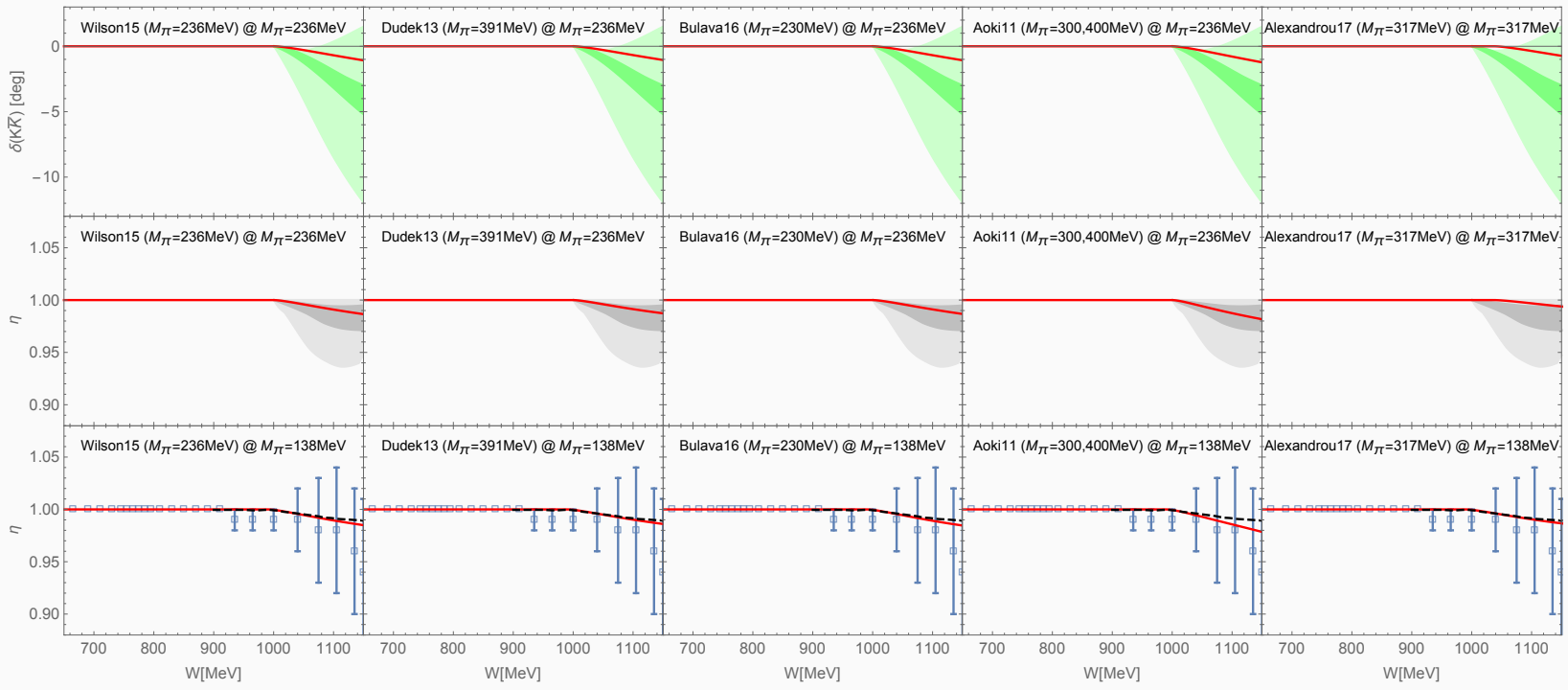

Figure 1: $K\bar{K}$ phase shifts (first row) and inelasticities (second row) obtained in the minimization for the different lattice data sets extrapolated at $m_\pi = 236$ MeV, in comparison with the result from [Wilson15] (bands). In the bottom row, the extrapolated inelasticity to the physical point, in comparison with the experimental data (squared), and with the Roy-Steiner solution (black-dashed lines).

Previous results with UChPT

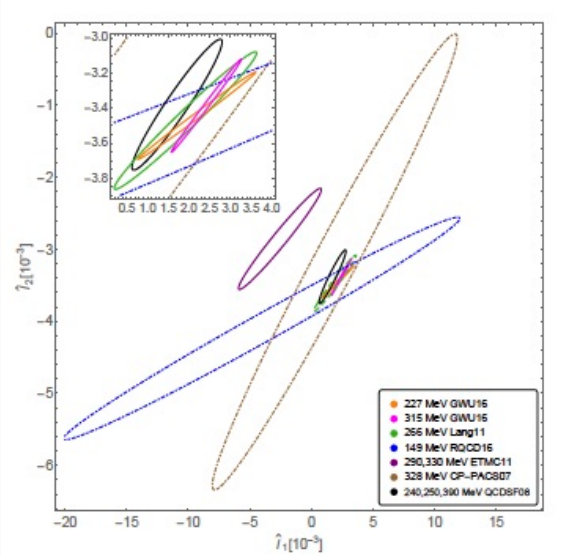

Figure 2: Error ellipses in the $(\hat{l}_1, \hat{l}_2)$ plane from SU(2) analyses.

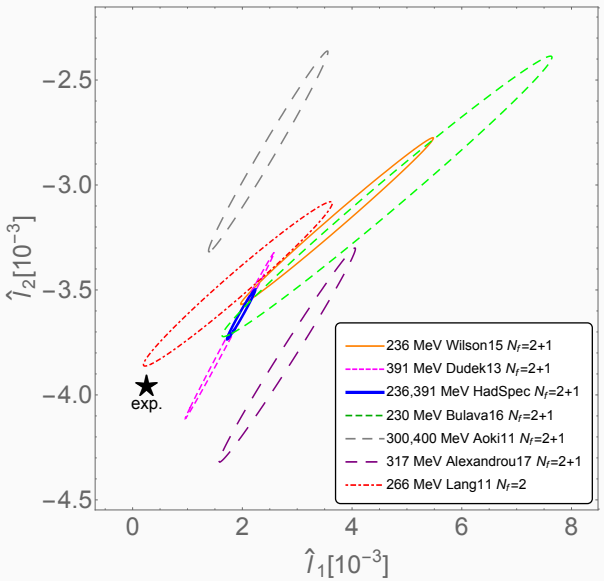

Figure 3: Error ellipses in the minimization for the SU(3) analyses.

While the SU(2) ellipses do overlap, the SU(3) ones, do not.

Previous results with UChPT

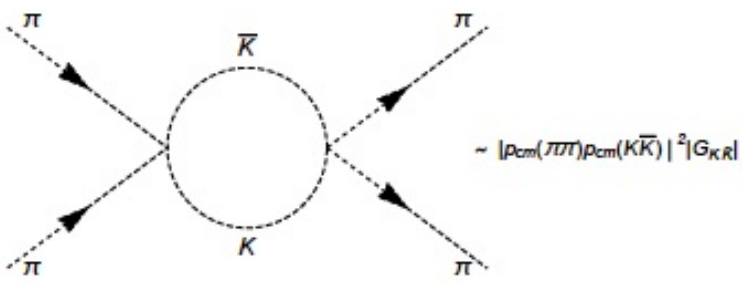

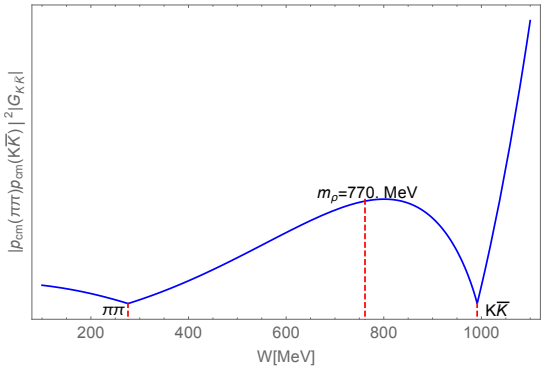

Ratio of the couplings of the ρ meson to $\pi\pi$ and $K\bar{K}$

	Oller/Pelaez(1999)	Guo/Oller(2012)
$\frac{g_{K\bar{K}}}{g_{\pi\pi}}$	0.54	0.64

Not that small!! NLO UChPT vs. One-loop UChPT

Motivation

Moreover....new available $N_f = 2 + 1$ data on different trajectories TrM$= K$: Andersen, Christian and Bulava, John and Hörz, Ben and Morningstar, Colin, Nucl. Phys. B(2018)

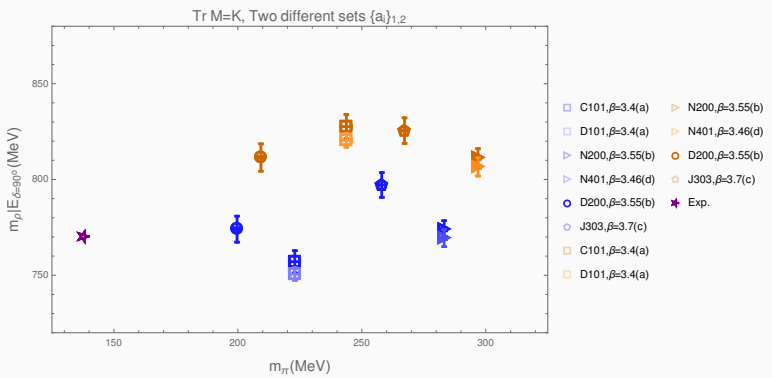

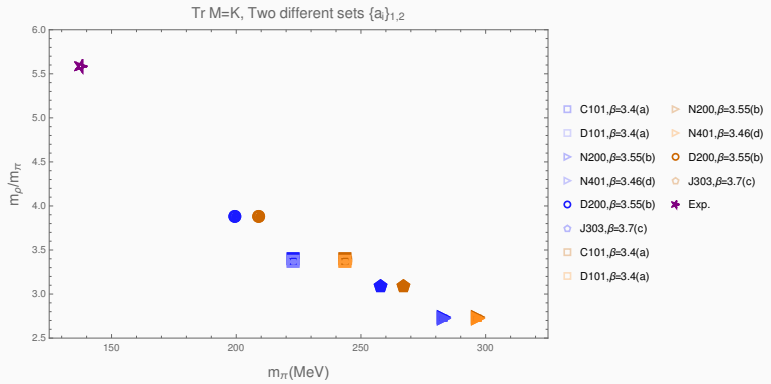

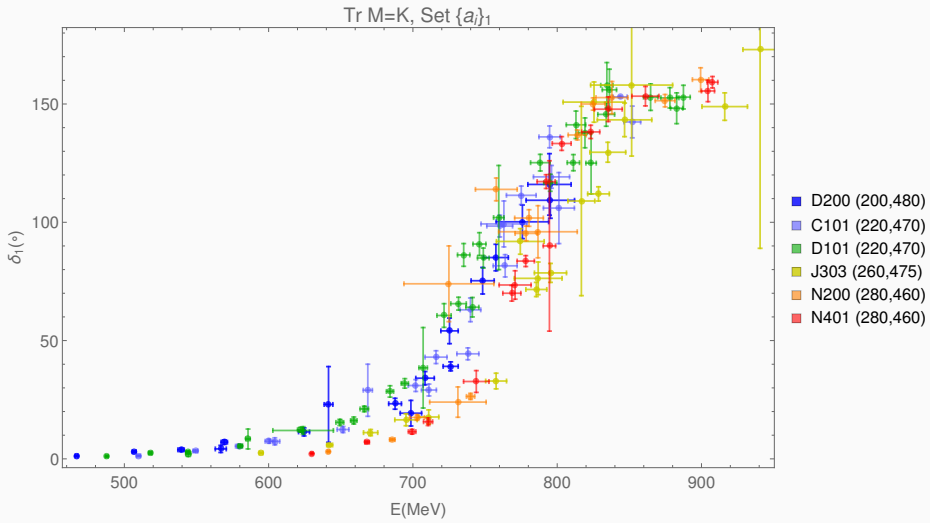

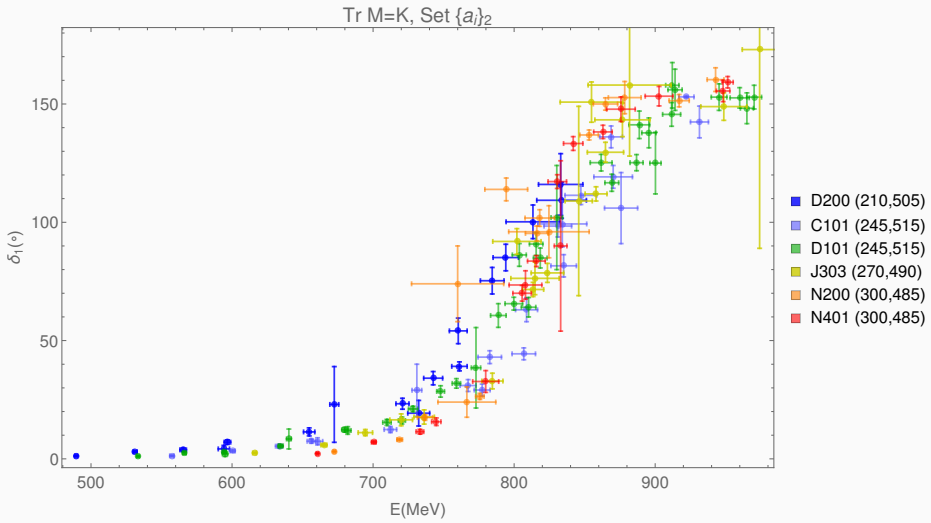

Can this be explained by different values of the strange quark (kaon) mass?

(or because of uncertainties in "a", or both...?)

Motivation

FLAG Review 2019

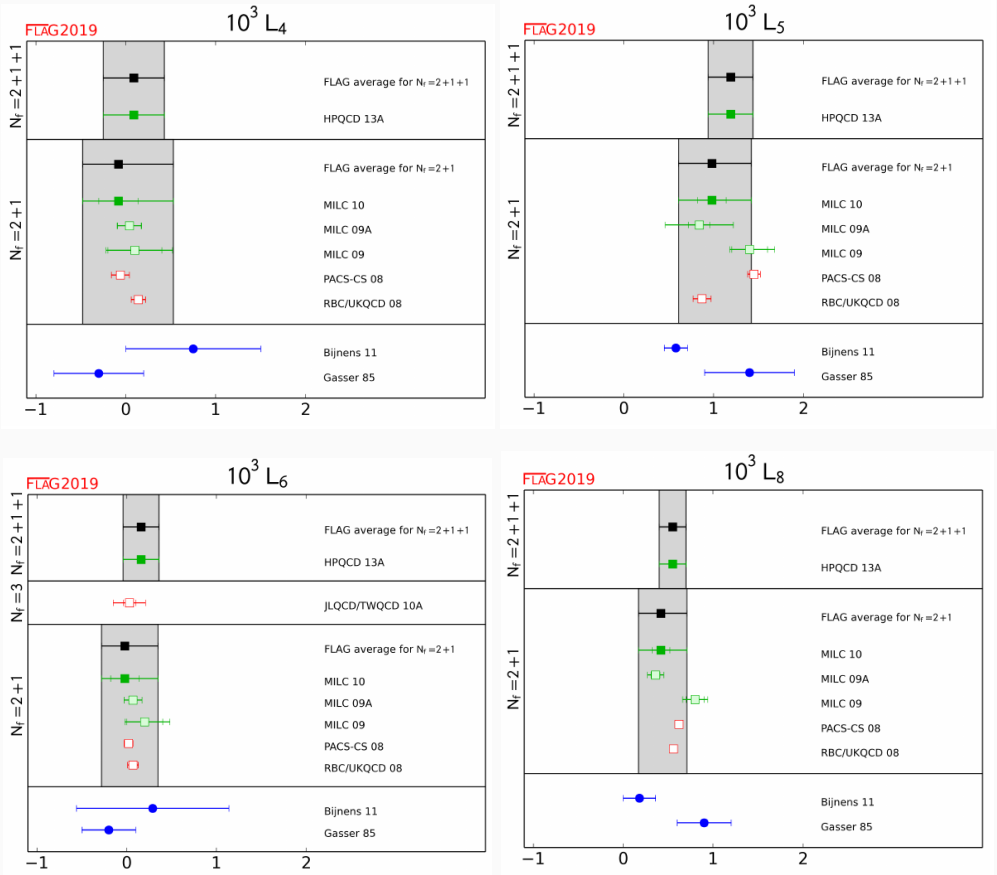

These LECs are only based on the trajectory $m_s = m_s^0$ ($0 \equiv$ phys.), no input on the strange quark mass dependence of decay constants.

The FLAG average is not a fit of data (large errors)

The LECs are a result of only decay constant data, f_π, f_K, analyses.

- Goldberger-Treiman Relation, $f_\pi = M_N g_A / g_{\pi NN}$
- Check of the KSFR relation, $g_{\rho\pi\pi} = m_\rho / \sqrt{2} f_\pi$

Strange quark mass dependence of the pseudoscalar decay constants and $\pi\pi$ phase shifts is still unknown

(and in particular for the ρ meson)

Inverse Amplitude Method

IAM in coupled-channels

$$\textbf{Unitarity} \quad \mathrm{Im}\, T^{-1} = -\Sigma\,, \quad \Sigma = \begin{pmatrix} \sigma_1 & 0 \\ 0 & \sigma_2 \end{pmatrix}\,, \tag{1}$$

$$T = T_2 \left[T_2 \mathrm{Re} T^{-1} T_2 - i\, T_2 \Sigma T_2 \right]^{-1} T_2\,, \Longrightarrow \boxed{T = T_2 [T_2 - T_4]^{-1} T_2} \tag{2}$$

Riemann sheet n,

$$T^{(n)}(s) = T(s) \left(\mathbb{1} + 2\, i\, \Sigma(s)^{(n)}\, T(s) \right)^{-1}\,, \tag{3}$$

$\pi\pi$, $K\bar{K}$ $I = J = 1$ coupled-channel system,

$$\Sigma^{II} = \begin{pmatrix} \sigma_1 & 0 \\ 0 & 0 \end{pmatrix}, \quad \Sigma^{III} = \begin{pmatrix} 0 & 0 \\ 0 & \sigma_2 \end{pmatrix}, \quad \Sigma^{IV} = \begin{pmatrix} \sigma_1 & 0 \\ 0 & \sigma_2 \end{pmatrix}\,.$$

$$\boxed{g_i g_j = -16\pi \lim_{s \to s_{\mathrm{pole}}} (s - s_{\mathrm{pole}})\, t_{ij} (2J+1)/2p^{2J}}, \tag{4}$$

Previous work $m_s = m_s^{(0)}$ trajectory, exper. phase shift data+lattice decay constant data: J. Nebreda and J. R. Pelaez., Phys. Rev. D (2010). f_P, m_P: NLO ChPT J. Gasser and H. Leutwyler, Annals Phys.(1984), Nucl. Phys. B(1985)

Chiral trajectories

- **Strange quark mass constant**, $m_s = k$:

$$M_{0K}^2 = +\frac{1}{2} M_{0\pi}^2 + k\, B_0 \ ,$$

where $k = m_s^{(0)}$ or $0.6\, m_s^{(0)}$.

- **Light and strange quark mass varies**, $\mathrm{Tr}\ \mathrm{M} = c$:

$$M_{0K}^2 = -\frac{1}{2} M_{0\pi}^2 + c\, B_0 \ ,$$

with $c = 2m_{ud}^{(0)} + m_s^{(0)}$. Predictions for other k's, c's, and:

- **Symmetric**, $m_s = m_{ud}$,

$$M_{0k}^2 = M_{0\pi}^2 \ ,$$

- **Light quark mass constant**, $m_{ud} = m_{ud}^{(0)}$,

$$M_{0\pi}^2 = M_{0\pi}^{2(0)}; M_{0K}^2 = M_{0K}^{2(0)} + (m_s - m_s^{(0)})\, B_0$$

Free parameters: $L_{12} = 2\, L_1 - L_2$ **and** L_i, $i = 3, 8$, **and** $c\, B_0$, $k\, B_0$, **adjusted to the the chiral trajectories.** $\mu = 770$ **MeV,** $f_0 = 80$ **MeV.**

Fitting procedure

- Energy measurements/phase shifts in the lattice are correlated:

$$\chi^2_W = (\vec{W}_1 - \vec{W}_0)^T C^{-1} (\vec{W}_1 - \vec{W}_0) \ , \tag{5}$$

$\vec{W}_0$: eigenenergies measured on the lattice,
C: covariance matrix,
$\vec{W}_1$:energies of the fit function. Inclined error bars in the $(W, \delta(W))$ plane, i. e., correlations from the Lüscher formula, $\delta_L = g(W)$, are considered reconstructing the energies, W_{1i}, from the fit function, $\delta_{\rm fit} = f(W_{1i})$, by means of a Taylor expansion near the measured energies W_{0i} (linear order), $\boxed{W_{1i} = \dfrac{g(W_{0i}) - f(W_{0i})}{f'(W_{0i}) - g'(W_{0i})} + W_{0i}}$

- Decay constants

$$\chi^2_f = \sum_{ij} (h_{ij} - h^l_{ij})^2 / e^{l\,2}_{ij} \tag{6}$$

where $i = 1, 3$ and $j = 1, n$, with n the number of data.
$h_1 = m_\pi / f_\pi$, $h_2 = m_K / f_K$ and $h_3 = m_K / f_\pi$.

Fitting procedure

$$\chi = \chi_W^2 + \chi_f^2 + \lambda \sum_{ij} \int |(S\,S^\dagger)_{ij} - \delta_{ij}|^2 \, dE \tag{7}$$

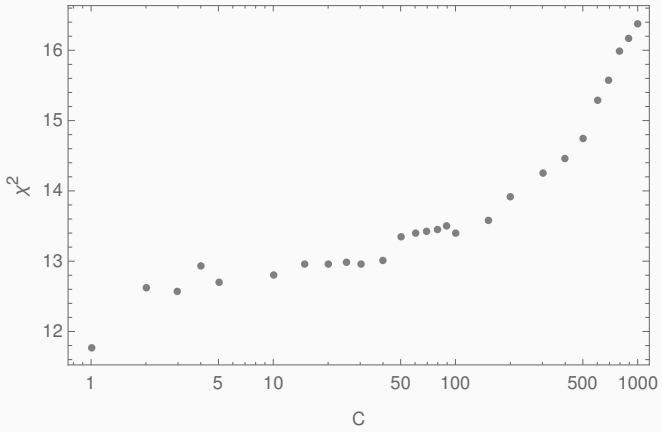

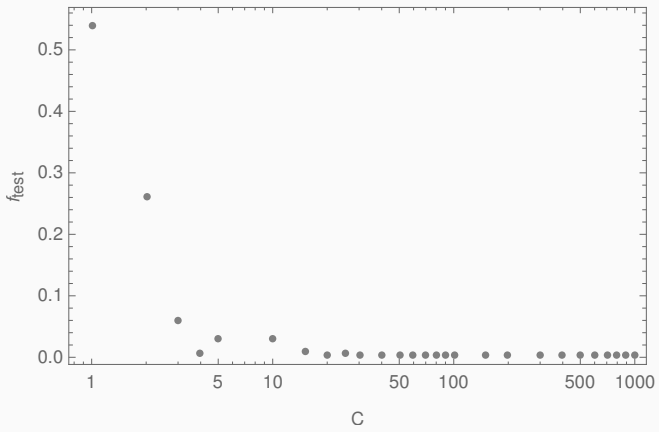

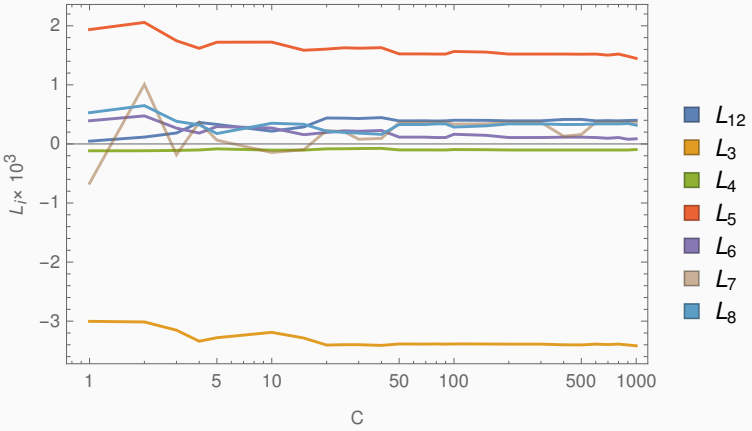

LECs which ensure unitarity,

$\lambda \simeq 30 - 40$

Results

Global fit to decay constants vs. decay constant + phase shifts

LEC$\times 10^3$	Fit I	Fit IV
L_{12}	-	0.36(3)
L_3	-	$-3.44(5)$
L_4	$-0.06(1)$	$-0.08(4)$
L_5	0.91(2)	0.98(6)
L_6	0.15(2)	0.25(9)
L_7	-	$-0.01(13)$
L_8	0.03(3)	0.1(1)

Table 1: Values of LECs in Fits I and IV.

Global fit to decay constants vs. decay constant + phase shifts

$c(k)\, B_0 \times 10^{-3} (\mathrm{MeV}^2)$	Fit I	Fit IV
$[c\, B_0]_{\beta=3.4}$	316(6)	266(16)
$[c\, B_0]_{\beta=3.55}$	295(6)	252(14)
$[c\, B_0]_{\beta=3.7}$	298(6)	255(14)
$[k\, B_0]_{m_{s,\mathrm{phys}}}$	257(6)	222(15)

Table 2: Values of parameters in Fits I and IV.

$\Sigma_0 = B_0 f_0^2 = -\langle 0|\bar{q}q|0\rangle_0 \Longrightarrow \boxed{\Sigma_0^{1/3} = 245 - 280 MeV}$

Flag review: 214 − 290 MeV.

MILC: $\Sigma_0^{1/3} = 245(5)(4)(4)$ MeV. We obtain 258 and 245 MeV for Fits I and IV in the $m_s = m_{s,\mathrm{phys}}$ trajectory, respectively, which are compatible.

Global fit to decay constants

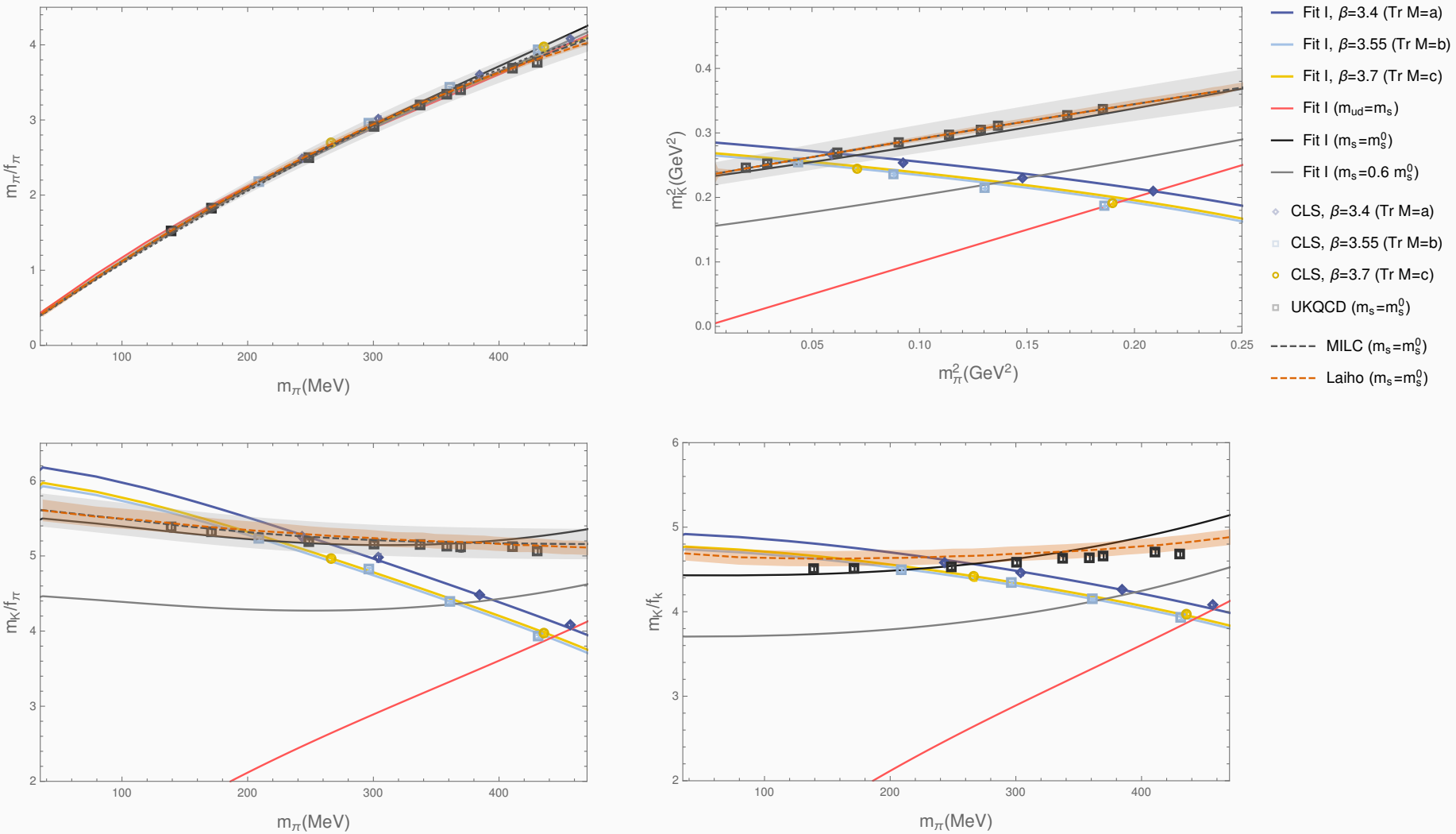

Figure 4: Chiral trajectories (top) and ratios m_π/f_π, m_K/f_π, and m_K/f_K obtained in fit I (decay constant data).

Chiral trajectories $m_s = k$

HS: rho phase shift data of HadSpec(236,391), JB: Bulava(235)
MILC,Laiho,UKQCD: decay constant data on $m_s = k$, $k = 0.6, 1\, m_{s,\mathrm{phys}}$. We find these data compatible (excludes JL/TWQCD, PACS-CS).

LEC$\times 10^3$	MILC,HS	UKQCD,HS	Laiho,HS	MUL,HS	Fit II
L_{12}	0.3(4)	−0.1(4)	0.1(2)	0.3(1)	0.2(1)
L_3	−3.4(4)	−3.1(4)	−3.4(2)	−3.4(1)	−3.4(1)
L_4	0.03(2)	0.04(1)	0.03(2)	0.05(2)	0.04(1)
L_5	1.2(2)	0.90(3)	0.90(5)	0.93(3)	0.94(2)
L_6	0.5(1)	0.24(3)	0.2(1)	0.25(4)	0.24(2)
L_7	0.6(3)	0.5(2)	0.5(1)	0.40(6)	0.44(6)
L_8	−0.5(1)	−0.3(1)	−0.2(1)	−0.3(1)	−0.27(4)

Table 3: Values of the LECs obtained from fits $m_s = k$.

Rho phase shift data on $m_s = k$

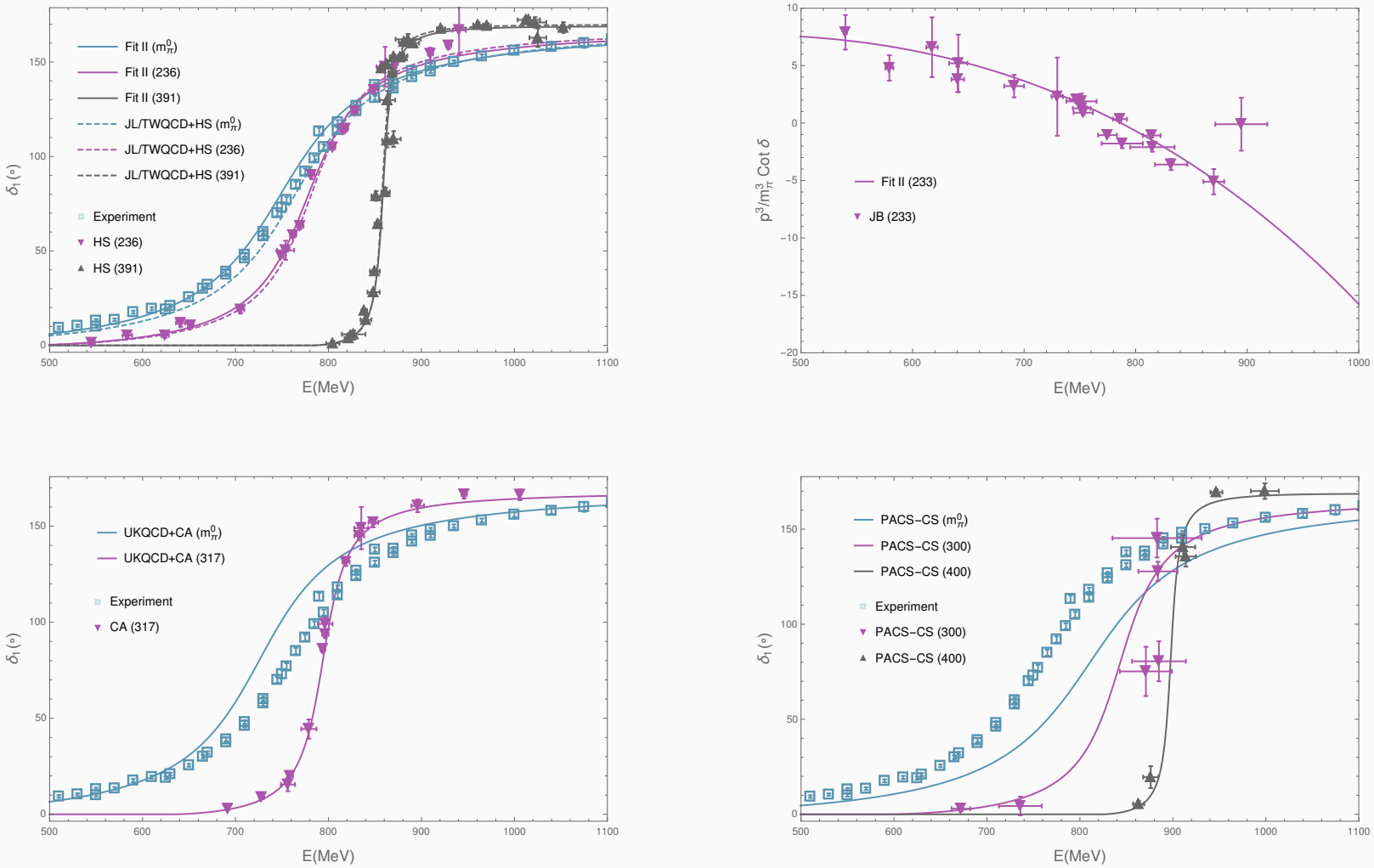

Figure 5: Phase shifts and extrapolations to the physical point from the fits in comparison with lattice and experimental data.

Similar findings than in PRD96 (2017) B. Hu, R. Molina and M. Döring et al.

Global fit decay constant + phase shift lattice data

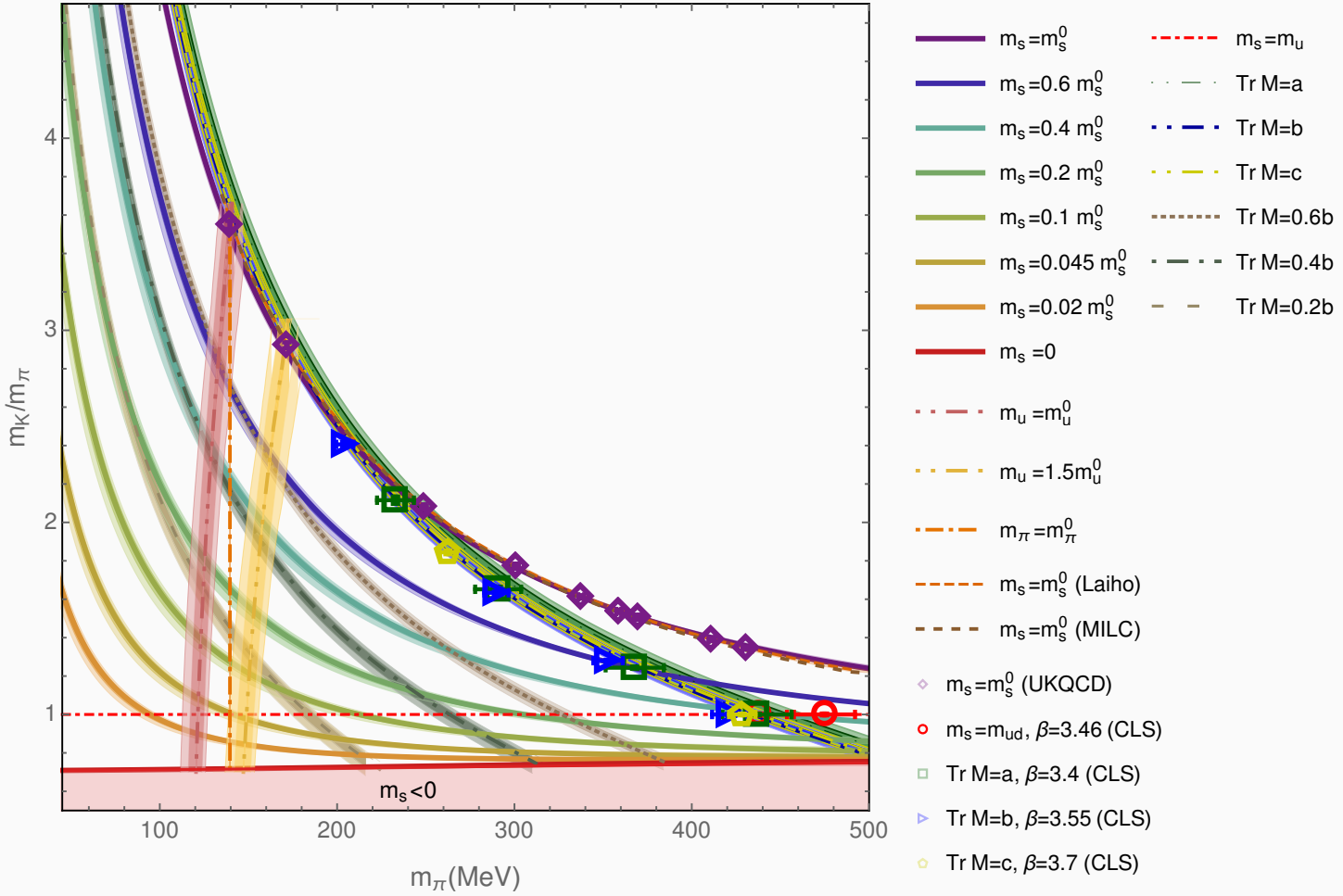

Errors evaluated with resampling over 300 fits, where the lattice enegies are variated with the same covariance matrices, phase shift data and also "$\{a_i\}$".

Global fit decay constant + phase shift lattice data

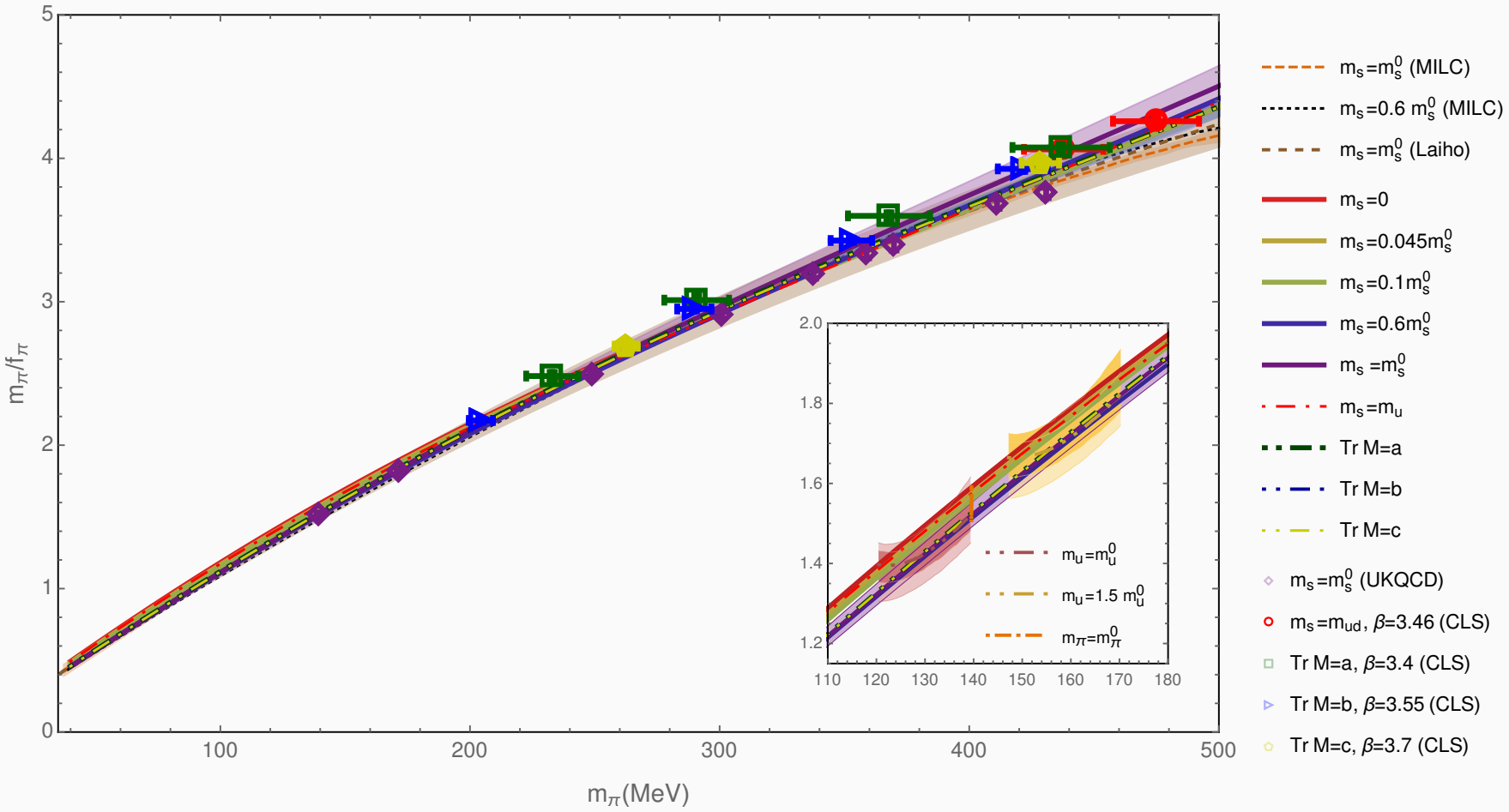

Figure 6: The ratio m_π/f_π as a function of m_π for different chiral trajectories, in comparison with the lattice data.

Global fit decay constant + phase shift lattice data

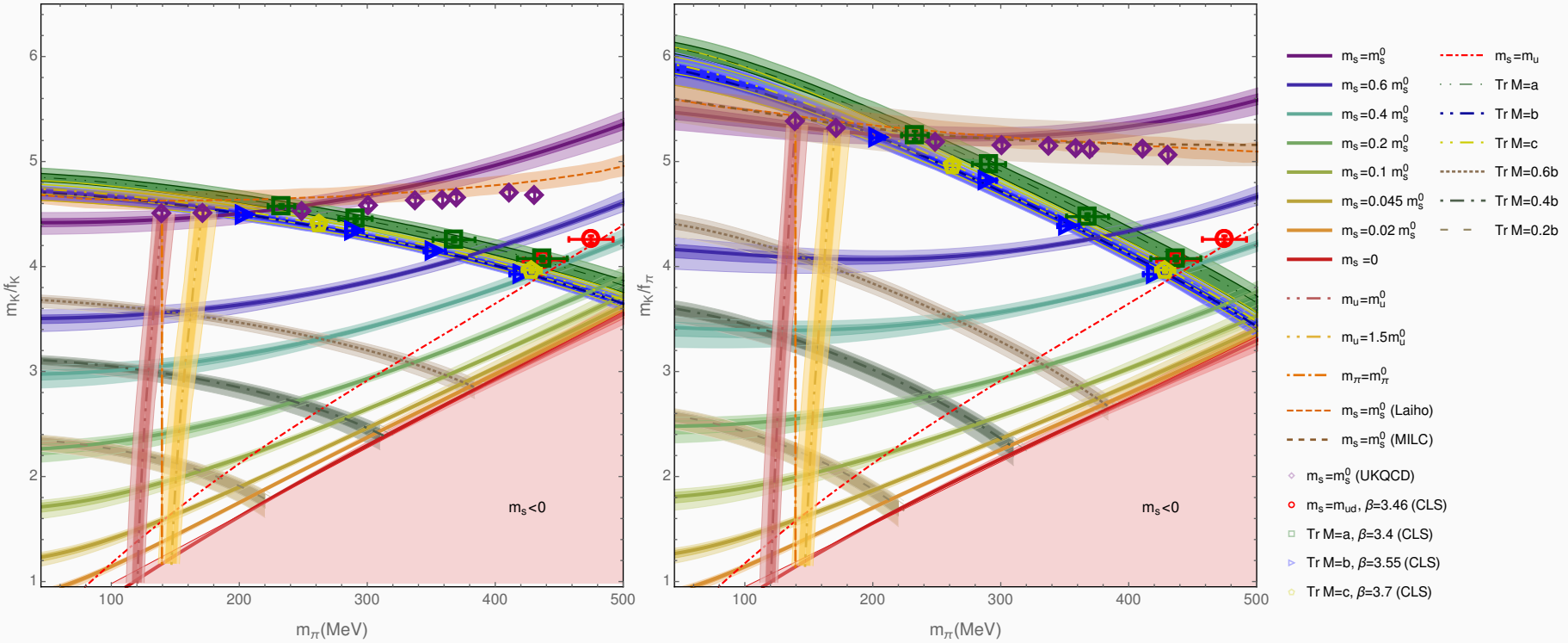

Figure 11: The ratios m_K/f_K and m_K/f_π as a function of m_π.

m_K^0/m_π^0	m_π^0/f_π^0	m_K^0/f_π^0	m_K^0/f_K^0
3.55(0.02)	1.51(0.012)	5.33(0.05)	4.45(0.04)

Table 4: Values of the ratios of pseudoscalar masses and decay constants extrapolated at the physical point as a result of fit IV.

Global fit decay constant + phase shift lattice data

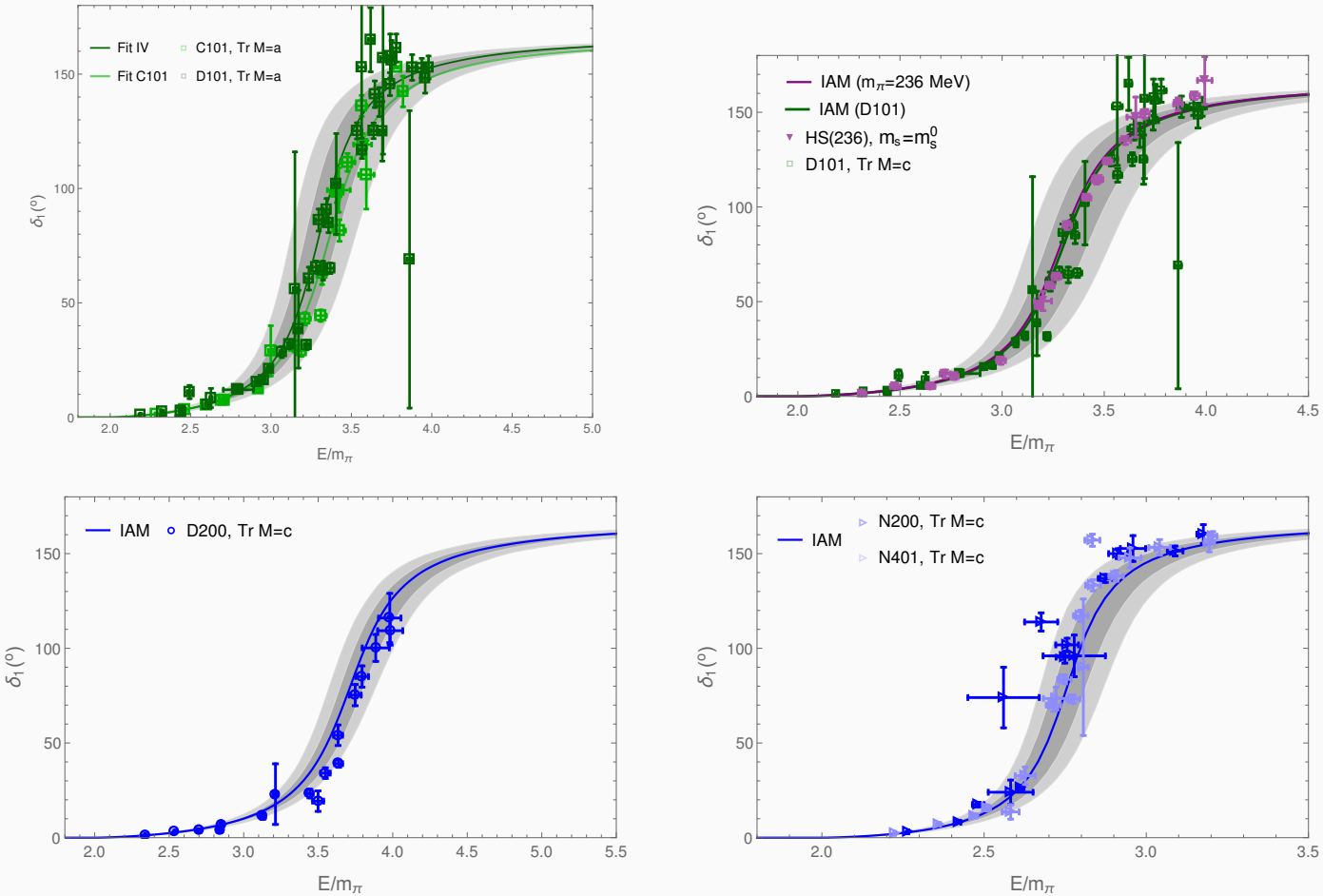

Figure 12: Phase shift lattice data for the trajectories Tr M= c in comparison with the result of the global fit ($m_\pi \simeq 200, 230$ and 280 MeV, D200, D101 and N200 respectively).

Global fit decay constant + phase shift lattice data

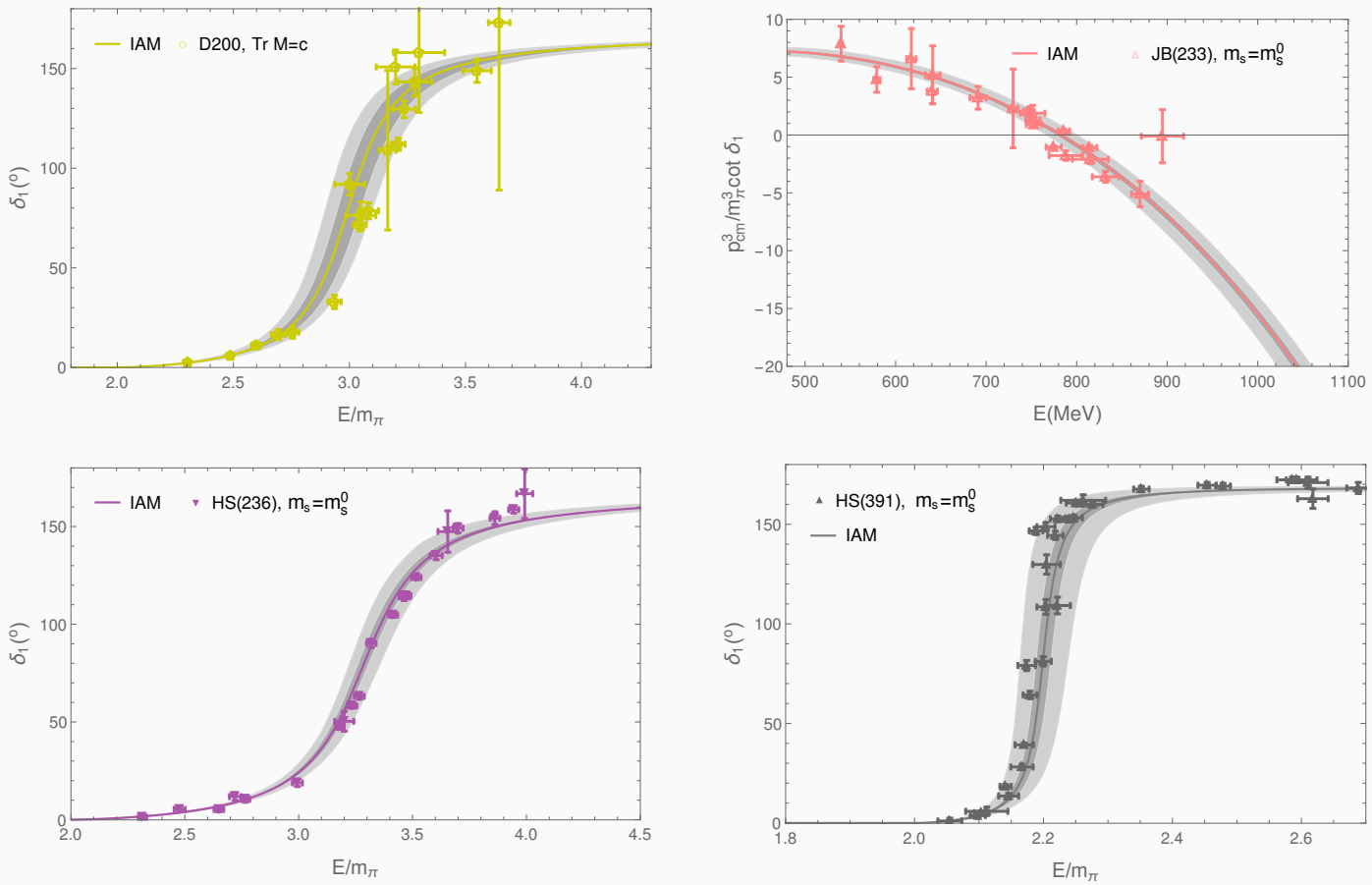

Figure 13: Phase shift lattice data for the trajectories Tr M= c ($m_\pi \simeq 260$ MeV), and $m_s = m_s^0$, in comparison with the result of the global fit.

Global fit decay constant + phase shift lattice data

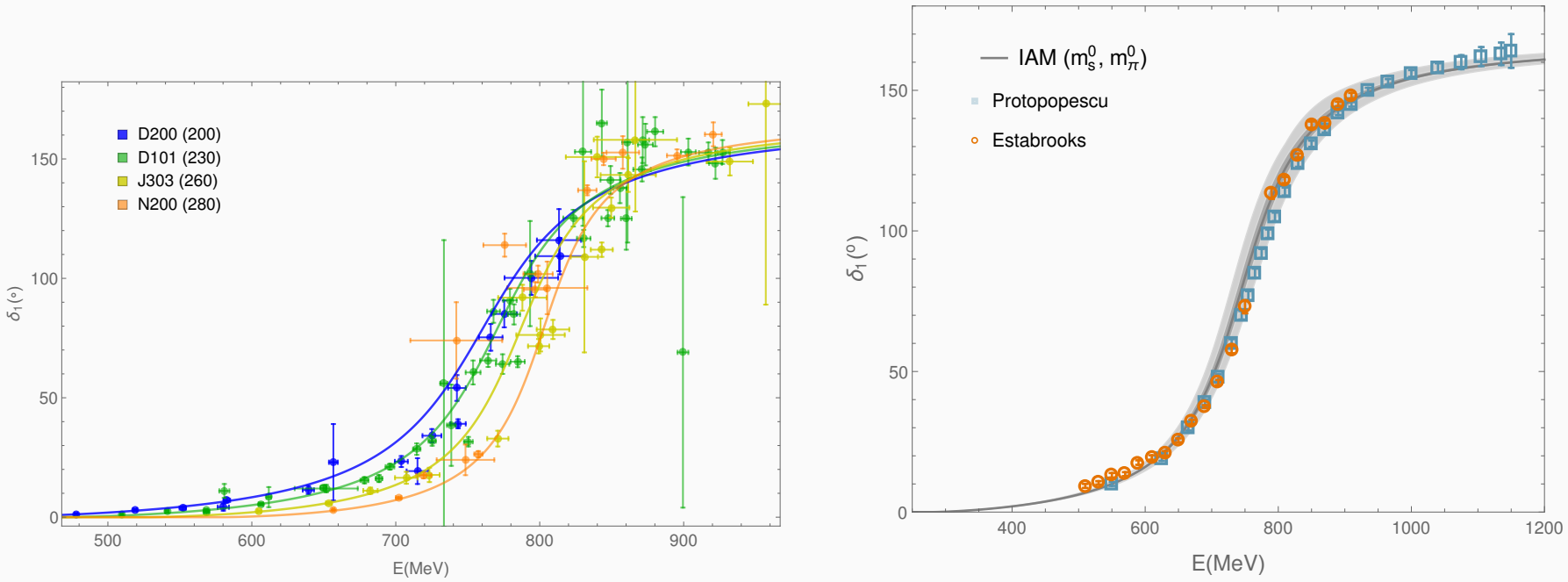

Figure 14: Phase shift lattice data for the trajectories Tr M= c, and extrapolation to the physical point in comparison with experimental data.

Global fit decay constant + phase shift lattice data

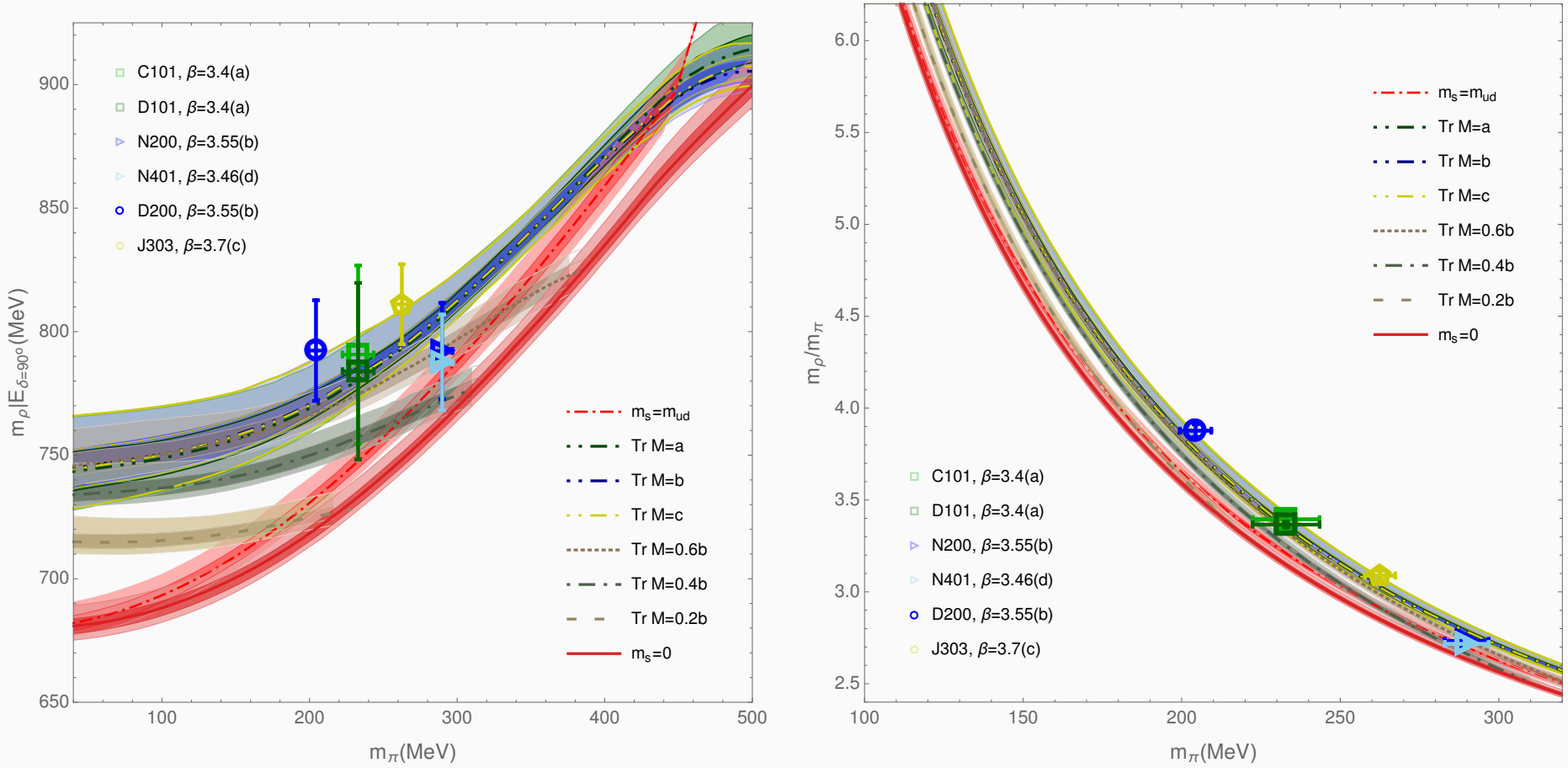

Figure 15: Result of the global fit for the trajectories Tr M= c, and in comparison with lattice data.

Global fit decay constant + phase shift lattice data

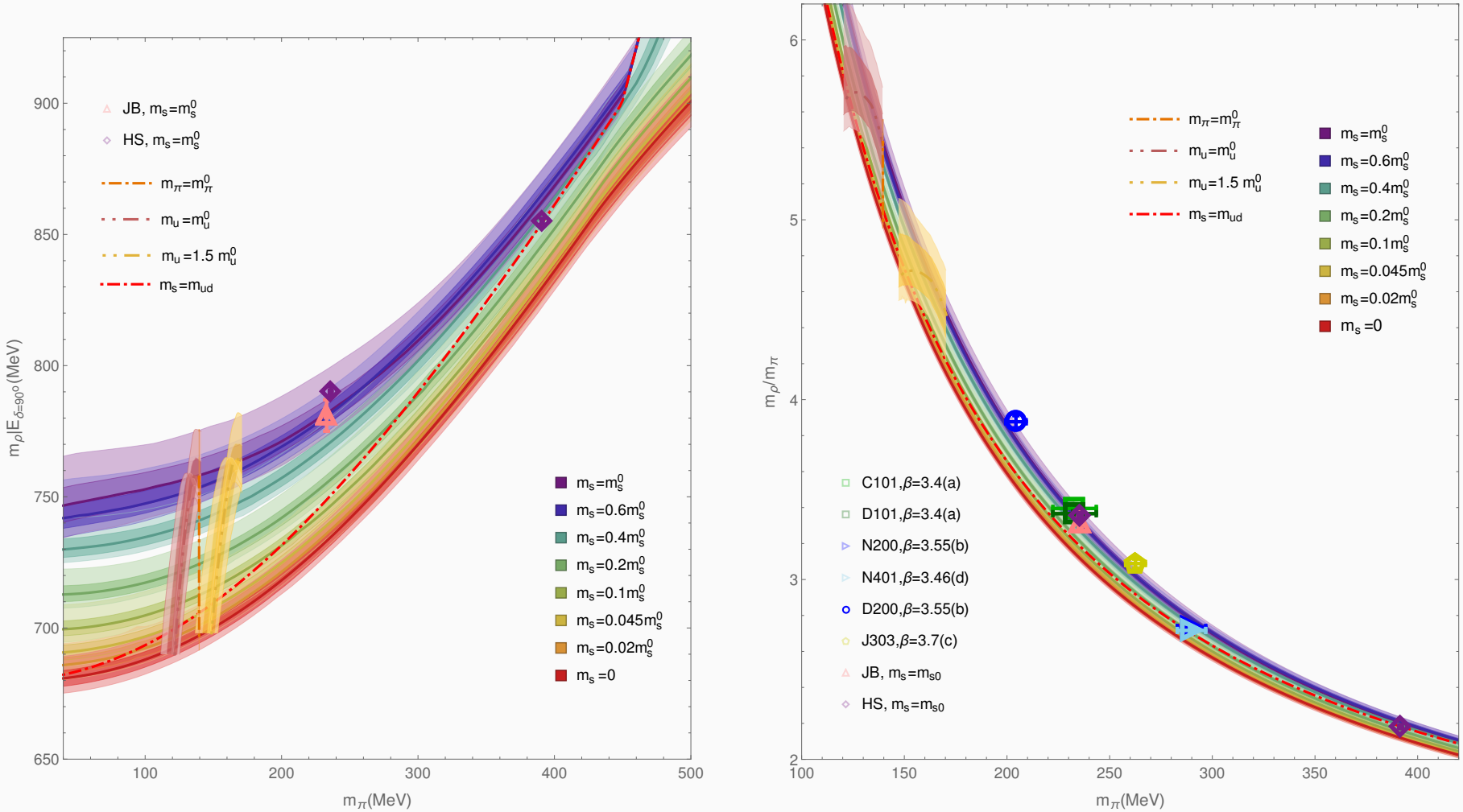

Figure 15: Result of the global fit for the phase shifts over trajectories $m_s = k$, and in comparison with lattice data.

Global fit decay constant + phase shift lattice data

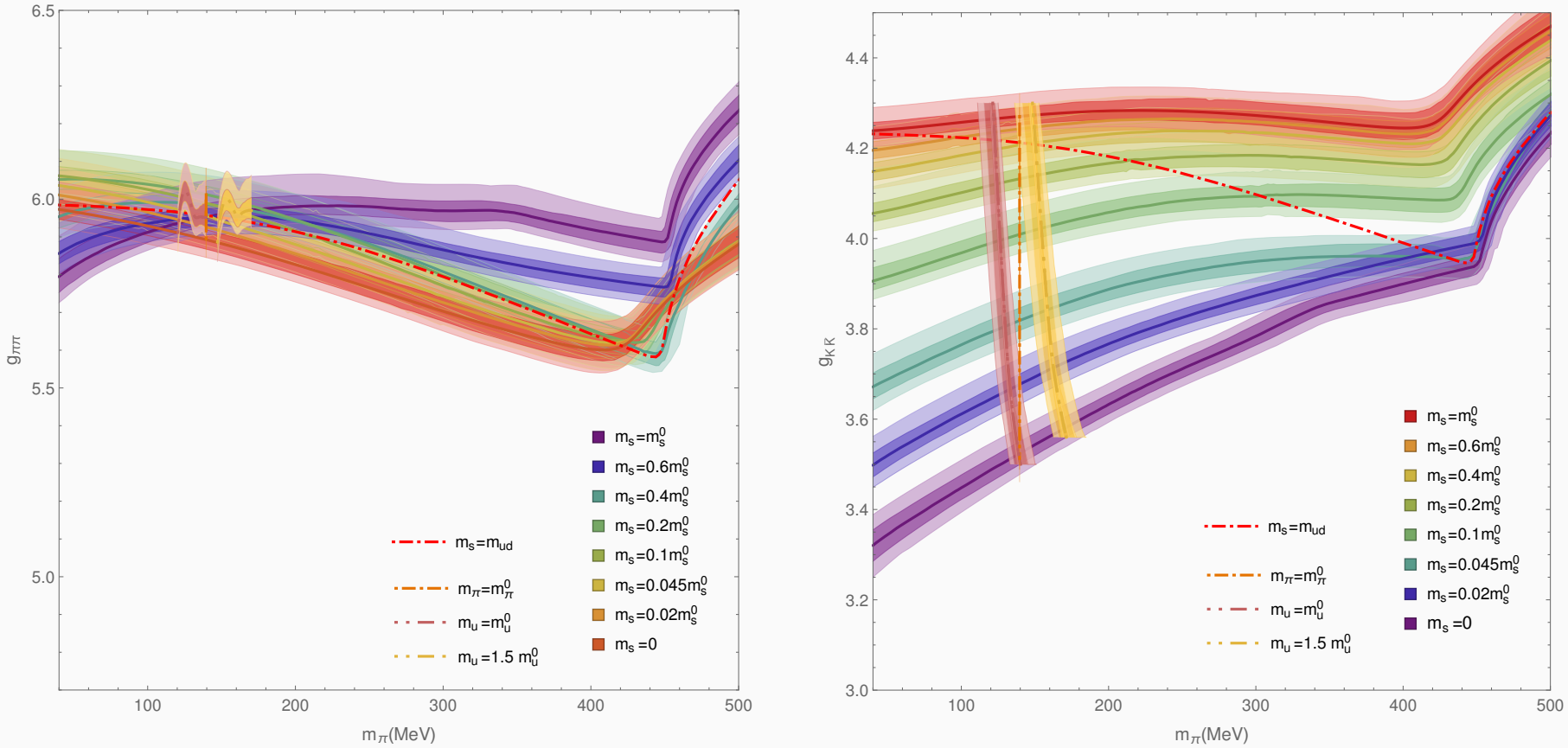

Figure 15: Result of the global fit for the coupling to $\pi\pi$ and $K\bar{K}$.

Global fit decay constant + phase shift lattice data

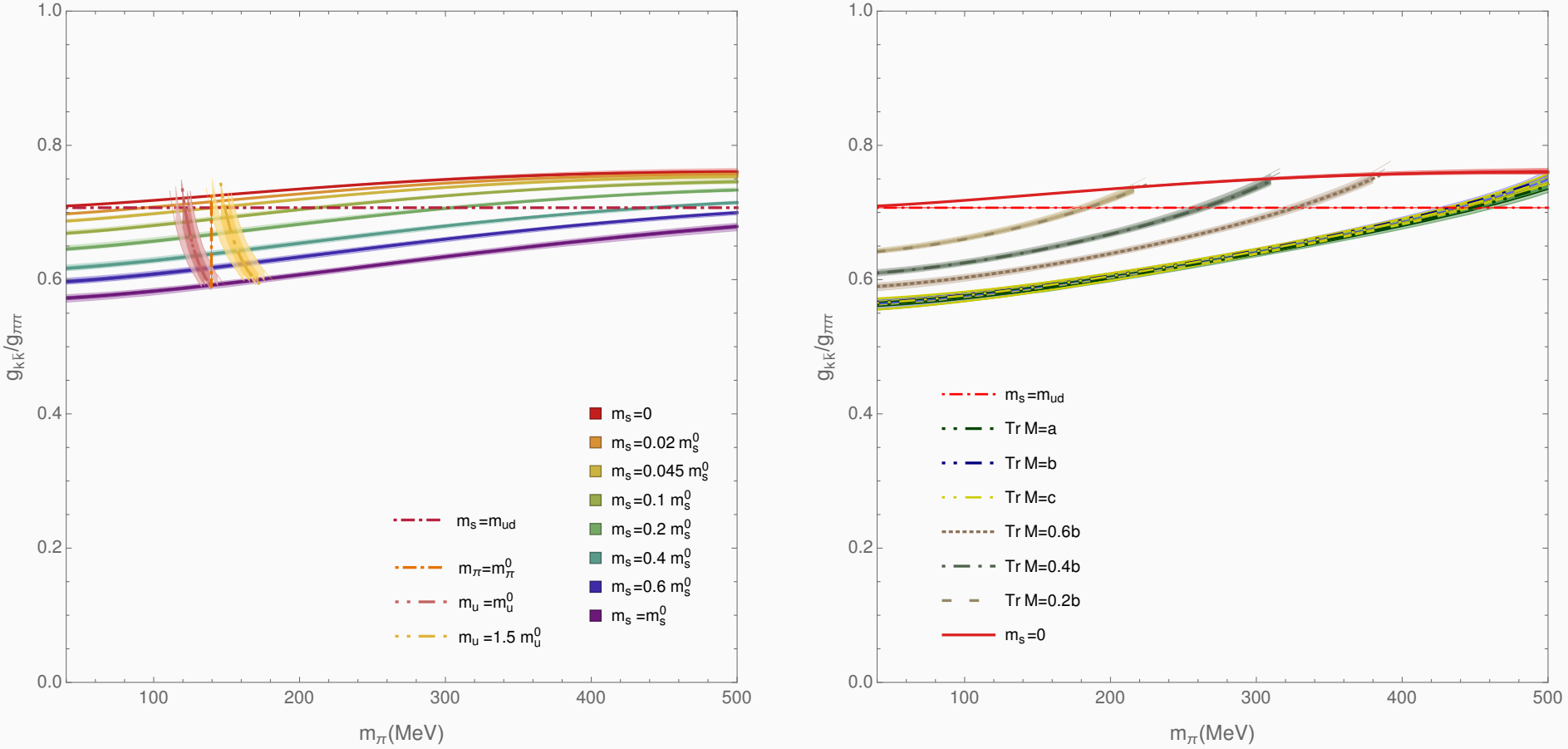

Figure 15: Result of the ratios for the couplings to $\pi\pi$ and $K\bar{K}$.

Global fit decay constant + phase shift lattice data

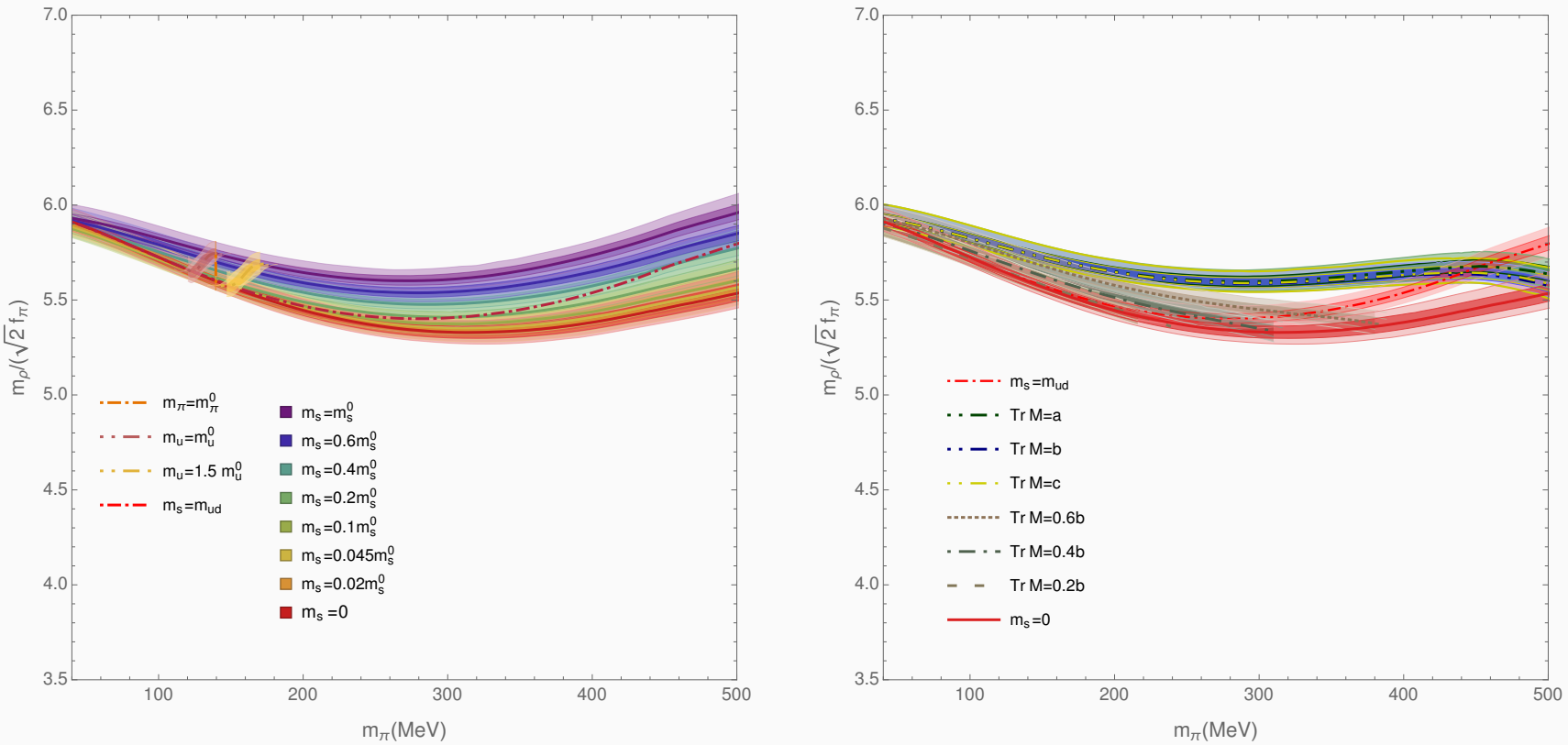

Figure 7: The rho mass divided by $\sqrt{2}f_\pi$ as a function of m_π and for different trajectories (KSFR).

Global fit decay constant + phase shift lattice data

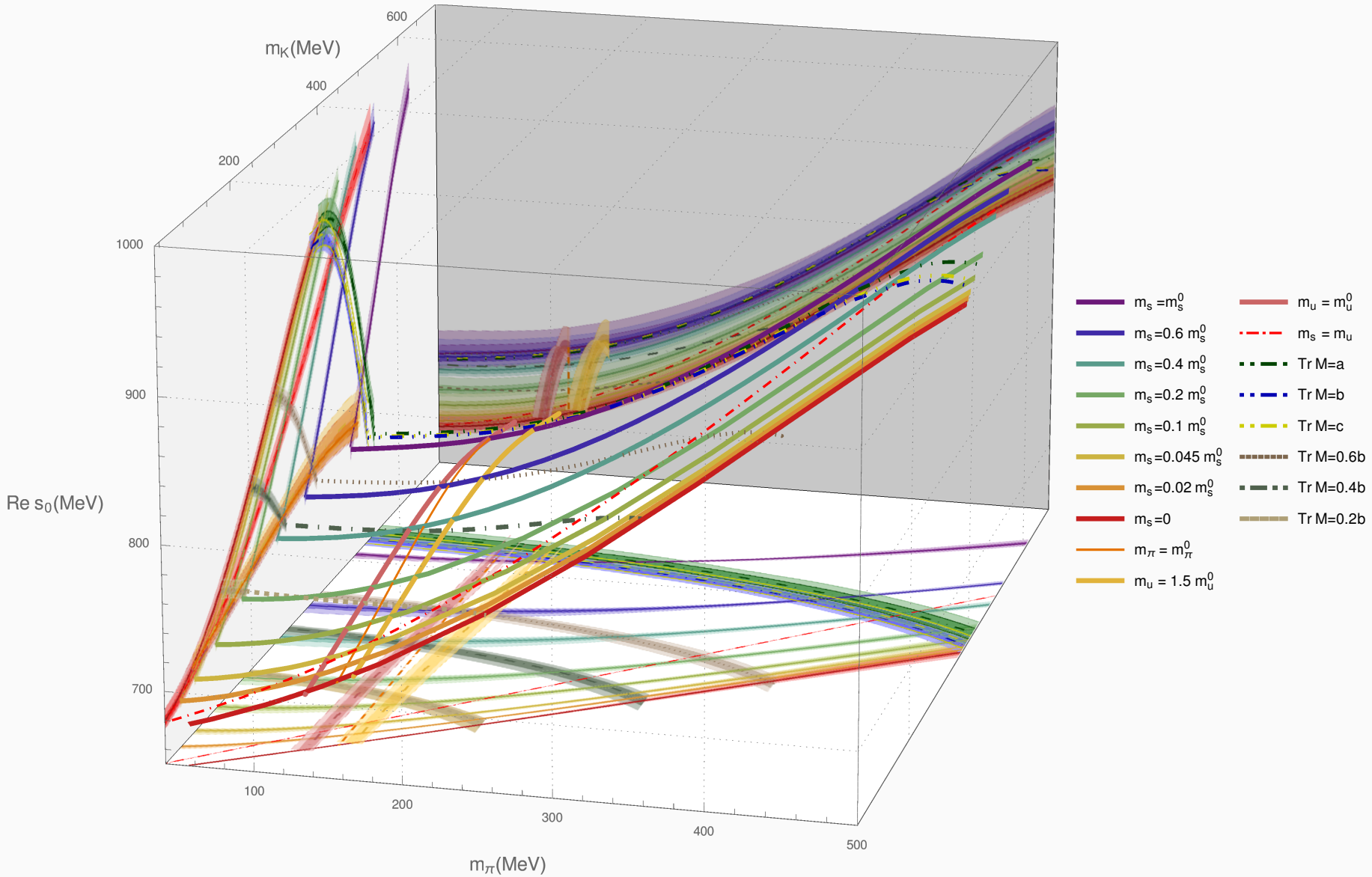

Figure 16: Real part of the pole position of the rho meson.

Global fit decay constant + phase shift lattice data

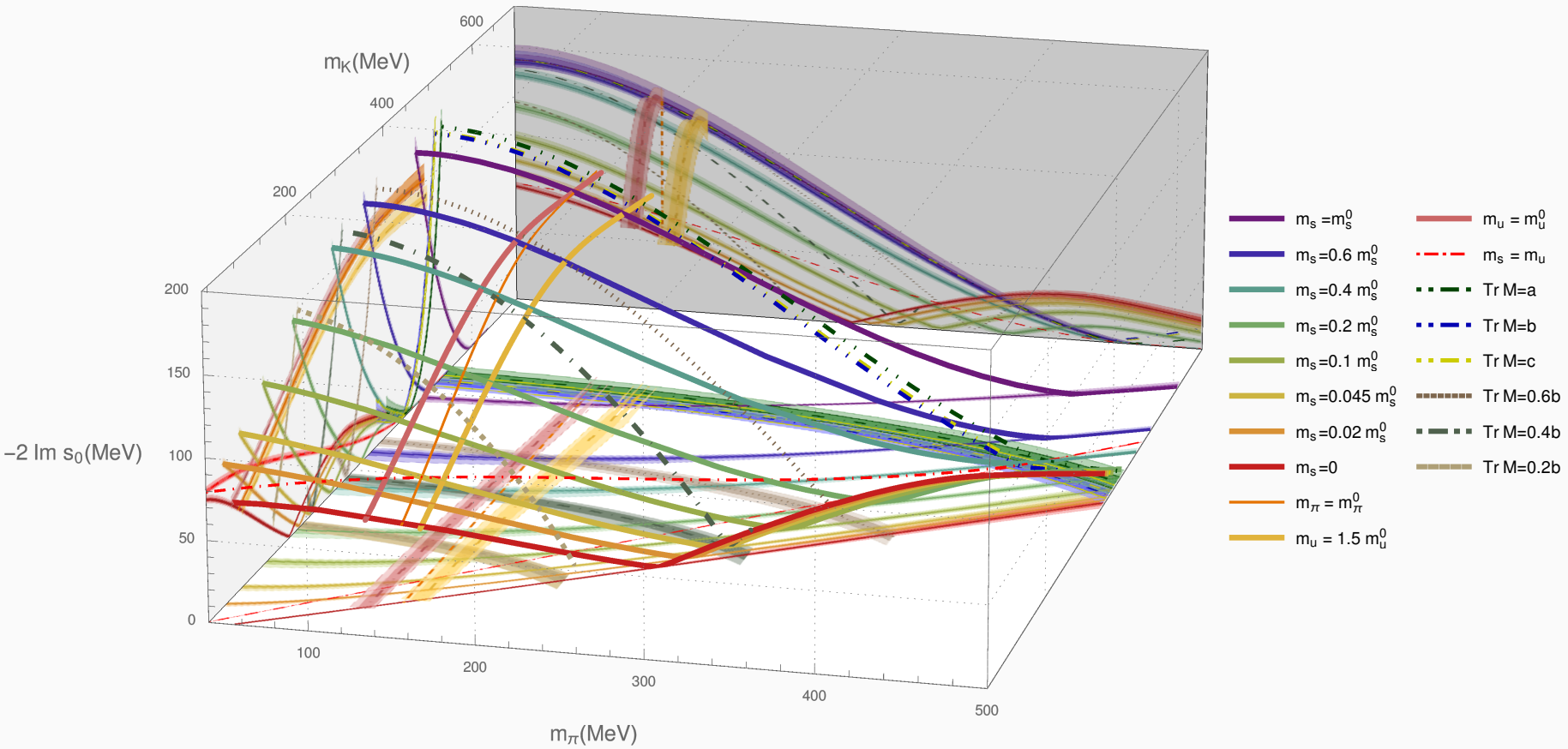

Figure 17: Decay width of the rho meson.

Global fit decay constant + phase shift lattice data

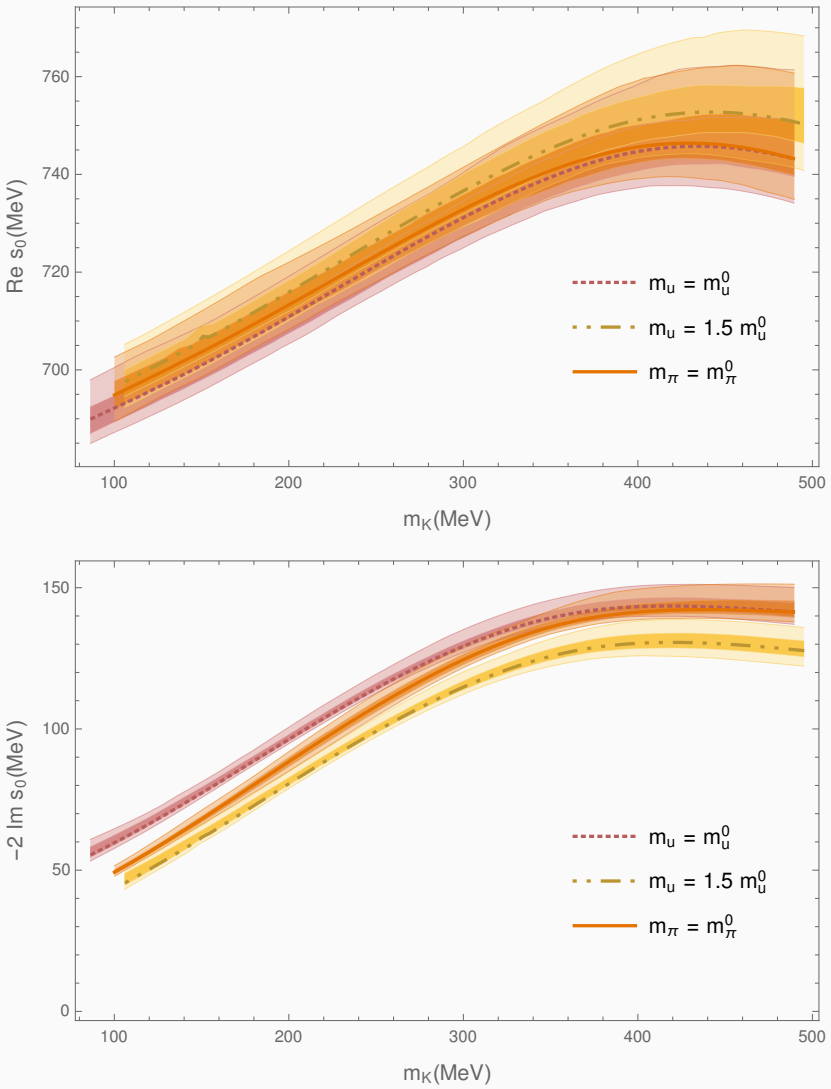

Figure 18: Mass and decay width of the rho meson in $m_{ud} = m_{ud}^0$, $m_{ud} = 1.5\, m_{ud}^0$ and $m_\pi = m_\pi^0$ trajectories.

Global fit decay constant + phase shift lattice data

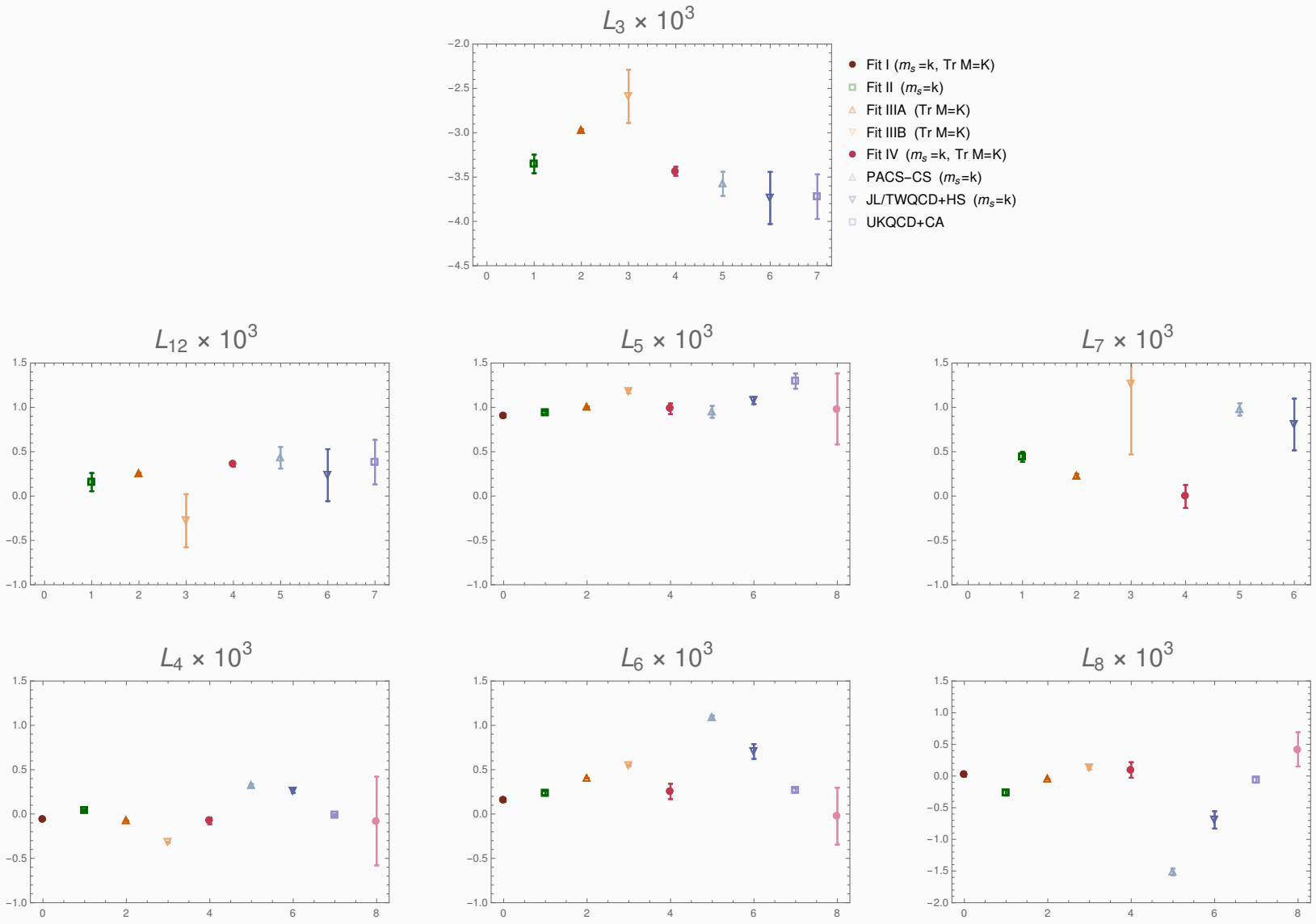

Figure 19: Values of the LECs obtained in the several combined and global fits in comparison with the FLAG average (pink).

Global fit decay constant + phase shift lattice data

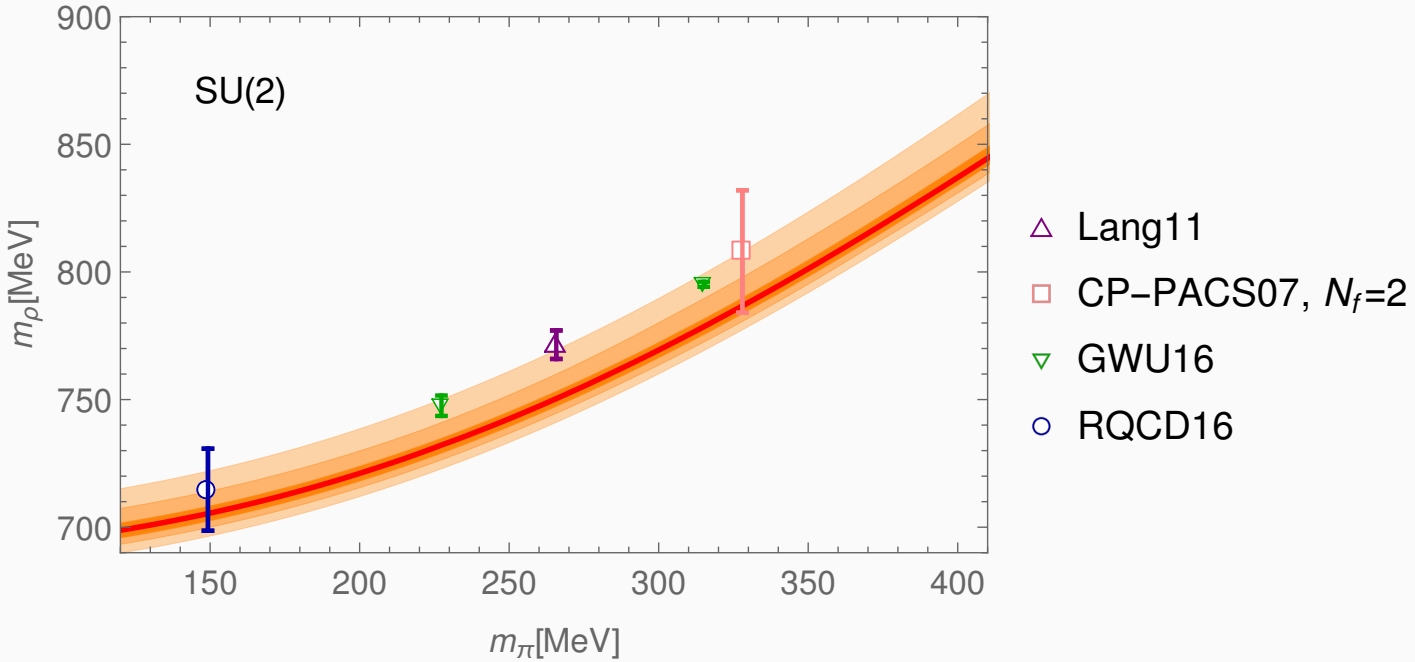

Figure 20: Mass of the rho meson when the $K\bar{K}$ interaction is dropped out.

Conclusions

Conclusions

- The strange quark plays a role in the $I = 1$ $\pi\pi$ scattering lattice simulations which becomes more relevant as it becomes lighter.
- The mass of the rho meson can be as light as 700 MeV for physical pion masses.
- In the symmetric line, the ratio of the couplings to $\pi\pi$ and $K\bar{K}$ is $\sqrt{2}$, due to the SU(3) Clebsch-Gordan coefficients.
- A transition is observed, around $m_\pi = 450$ MeV, where the rho meson in the simulations becomes bound in the $m_s = k$ trajectories, while it becomes a resonance decaying to $K\bar{K}$ in the Tr M$= c$ curves.

NLO Chiral Perturbation Theory

Masses

$$M_\pi^2 = M_{0\,\pi}^2 \left[1 + \mu_\pi - \frac{\mu_\eta}{3} + \frac{16 M_{0\,K}^2}{f_0^2}(2L_6^r - L_4^r) + \frac{8 M_{0\,\pi}^2}{f_0^2}(2L_6^r + 2L_8^r - L_4^r - L_5^r)\right],$$

$$M_K^2 = M_{0\,K}^2 \left[1 + \frac{2\mu_\eta}{3} + \frac{8 M_{0\,\pi}^2}{f_0^2}(2L_6^r - L_4^r) + \frac{8 M_{0\,K}^2}{f_0^2}(4L_6^r + 2L_8^r - 2L_4^r - L_5^r)\right]$$

$$M_\eta^2 = M_{0\,\eta}^2 \left[1 + 2\mu_K - \frac{4}{3}\mu_\eta + \frac{8 M_{0\,\eta}^2}{f_0^2}(2L_8^r - L_5^r) + \frac{8}{f_0^2}(2M_{0\,K}^2 + M_{0\,\pi}^2)(2L_6^r - L_4^r)\right]$$
$$+ M_{0\,\pi}^2 \left[-\mu_\pi + \frac{2}{3}\mu_K + \frac{1}{3}\mu_\eta\right] + \frac{128}{9 f_0^2}(M_{0\,K}^2 - M_{0\,\pi}^2)^2(3L_7 + L_8^r),$$

Decay constants

$$f_\pi = f_0 \left[1 - 2\mu_\pi - \mu_K + \frac{4 M_{0\,\pi}^2}{f_0^2}(L_4 + L_5) + \frac{8 M_{0\,K}^2}{f_0^2} L_4\right],$$

$$f_K = f_0 \left[1 - \frac{3\mu_\pi}{4} - \frac{3\mu_K}{2} - \frac{3\mu_\eta}{4} + \frac{4 M_{0\,\pi}^2}{f_0^2} L_4 + \frac{4 M_{0\,K}^2}{f_0^2}(2L_4 + L_5)\right],$$

$$f_\eta = f_0 \left[1 - 3\mu_K + \frac{4L_4}{f_0^2}\left(M_{0\,\pi}^2 + 2M_{0\,K}^2\right) + \frac{4 M_{0\,\eta}^2}{f_0^2} L_5\right].$$